Improving Operational Accuracy of a Mobile Manipulator by Modeling Geometric and Non-Geometric Parameters

Thanh D V Nguyen, Vincent Bonnet, Pierre Fernbach, Thomas Flayols, Florent Lamiraux

Improving Operational Accuracy of a Mobile Manipulator by Modeling Geometric and Non-Geometric Parameters

Thanh D. V. Nguyen[1,2,*], Vincent Bonnet[1,3], Pierre Fernbach[2], Thomas Flayols[1], Florent Lamiraux[1]

***Abstract*— This paper aims to address two intrinsic phenomena encountered in mobile manipulator robots, but often neglected, with the objective of improving the overall accuracy of end-effector pose estimation. Firstly, after performing state-of-the-art geometric calibration of the arm, we propose two identifiable mathematical models to account for non-geometric effects: a model for the mobile base suspension system and a model of non-linear inaccuracies of joint angles estimates. The latter is due to backlash and misaligned encoders mounting. Then, the proposed models were experimentally validated on the mobile manipulator TIAGo using a stereophotogrammetric system. Overall, the end-effector pose accuracy was improved by 60% when compared to the nominal manufacturer model, with root mean square errors (RMSE) of 5.7mm and 2.7deg for positional and orientational errors, respectively.**

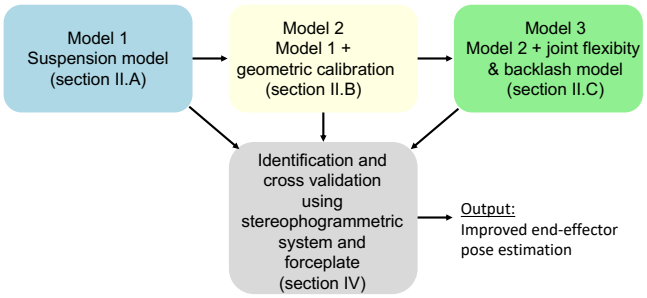

Fig. 1. Overview of the models proposed for improving mobile manipulator accuracy.

I. INTRODUCTION

The agility and adaptability of mobile base collaborative robots make them invaluable assets in real-life applications ranging from manufacturing to healthcare. However, their relatively light and often inexpensive construction could compromise their operational accuracy, posing significant challenges in applications requiring accurate and precise positioning and manipulation. The inaccurate positioning prediction issues faced by mobile base collaborative robots could be caused by various factors. Notably, these include the absence of proper geometric calibration, where users often over-rely on the geometric specifications initially provided without re-calibrating after extended usage [1]. Furthermore, in many cases, imperfect manufacturing or natural degradation can significantly impact the performance of mobile manipulators. The lack of accountability for these unmodeled phenomena can also contribute to worsened accuracy. Among the deteriorating behaviors in mobile manipulators, the most critical ones include the undesired backlash in mechanical transmission gears, the unknown dynamics of the base suspension, the joint flexibility, and occasionally the misaligned mounting of encoders at the joint. It is essential to address all of these phenomena for achieving an efficient operational performance with mobile manipulators. In the existing literature, researchers have offered solutions aimed at enhancing the operational accuracy of mobile manipulators, focusing primarily on refining kinematic models through experimental methods such as hand-eye calibration [2], fusion of camera measurements with 2D lidar [1], and self-calibration using measured contact data with point cloud registration [3]. However, to the authors' knowledge, there has been minimal exploration of other structural issues, such as those mentioned previously, which could also have a significant impact on the mobile manipulator accuracy. Consequently, it is evident that there exists a gap in the current research pertaining to these aspects.

A robotic system comprises rigid links interconnected by joints, with a drive motor transferring power through gears. When there is a clearance between mating gear teeth, backlash occurs. While a certain mount of backlash can be crucial for smooth movement, it can also increase with gear wear, eventually leading to transmission disruptions and inaccuracies in end-effector positioning. In the field of mechanics, the study of backlash has been thoroughly conducted with various proposed models as well as experimental verification methods. For instance, studies by Sakkar et al. [4], which analyzed joint output torque using a torque sensor, and by Stein et al. [5], which examined output speed using a mounted tachometer, emphasized the analysis of impact-vibration. They noted that the contact between gear teeth could disturb the measured output signal in speed or joint torque, leading to the inference of backlash detection and estimation. In robotics, backlash investigation has been limited to some specific use cases of industrial manipulators. Slamani et al. [6] proposed a polynomial-based approximation for backlash estimation at the tool center point, rather than modeling backlash at each individual joint of an industrial manipulator. Other studies have modeled and identified backlash as a contributing factor to the elastic behavior of robot joints, alongside friction and hysteresis [7]. Additionally, Giovannitti et al. [8] introduced an innovative method for estimating backlash using only encoders by analyzing the disturbances caused by stimulated movement. These results were obtained

[1] LAAS-CNRS, Université Paul Sabatier, CNRS, Toulouse, France
[2] TOWARD S.A.S, Toulouse, France
[3] Image and Pervasive Access Laboratory (IPAL), CNRS-UMI, 2955, Singapore
[*] corresponding author: dvtnguyen@laas.fr
This work was partially supported by PAL Robotics

through experimentation of industrial manipulators where the amount of backlash is extremely small compared to that of mobile manipulators. For light weight robots such as mobile manipulators, not only gear backlash but also misaligned encoders mounting have unfortunately not been given proper consideration. Even though, the eccentricity of a rotary absolute encoder due to the misalignment can lead to a periodic non-linear measurement error [9] which directly affecting the reliability of measurements, this phenomenon has not been considered seriously in calibration process for robots. Quantifying these errors altogether can certainly improve the operational accuracy of mobile manipulators.

In most mobile manipulators, suspension systems are intrinsic components designed to withstand different terrains. These suspension systems can be either carefully designed with springs and dampers or presented in the form of compliant elements such as tires. The identification of suspension models in robotics remains largely unexplored. Notable exceptions include Sujan et al. [10], who investigated suspension dynamics of a rover for rough terrain exploration. Their approach involved using a joint torque sensor and an inclinometer to virtually identify a generalized 6D spring-damper model. However, their results were limited since the experiment was restrained by observability constraints of their sensor options. A more comprehensive study would offer benefits and applicability.

In this context, we propose a procedure to improve operational accuracy by considering both geometric and non-geometric phenomena in modeling a mobile manipulator robot. Hypothesized models are first investigated and formulated for the base suspension system, the gear backlash and other non-geometric phenomena at the joint level. Experimentation on the mobile manipulator robot TIAGo will demonstrate these behaviors as well as validate the hypothesized models in isolated manner, and in integrated manner with a geometric calibration process to verify the overall effectiveness on improving the operational accuracy. Finally, results from experimentation will be discussed.

II. Methods

This paper proposes to analyze the contribution to the end-effector pose accuracy of a mobile manipulator robot of three causes: the geometric parameters, the effect of the suspension at the robot base, and backlash, joint flexibility, and misaligned encoder mounting. As described in Fig. 1 four models were developed:

- **Nominal model**: The nominal geometric model provided by the robot manufacturer, i.e. without any calibration performed.
- **Model 1**: This model includes a suspension model at the robot base.
- **Model 2**: This model includes the suspension model at the robot base and the full-kinematic calibrated model.
- **Model 3**: This model includes the suspension model at the robot base, the full-kinematic calibrated model, and the model of the gear backlash and non-geometric phenomena.

The base of the TIAGo robot features six wheels: two driving wheels and four supporting caster wheels, as depicted in Fig. 3.a. First, let us denote the following frames to formulate our problem: the world frame as $\mathscr{F}_0$, the frame attached to the robot as $\mathscr{F}_r$, where $\mathscr{F}_0$ and $\mathscr{F}_r$ are identically located at the base link of the robot in its resting state, as illustrated in Fig. 3.b, the wheel frame $\mathscr{F}_{w_i}$ with $i = \{1, ..., 6\}$ for each of six wheels. In addition, we also define the measurement frames as following: the reference frame of measurement system $\mathscr{F}_m$, the measurement frame attached to the robot base $\mathscr{F}_b$, the measurement frame attached to the robot shoulder $\mathscr{F}_s$, and the measurement frame attached to the robot gripper $\mathscr{F}_g$, as illustrated in Fig. 2.

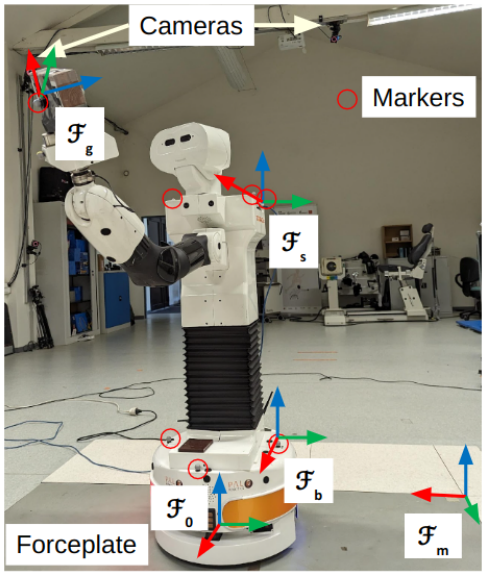

Fig. 2. Frames definition and experimental setup.

A. Suspension Model Identification

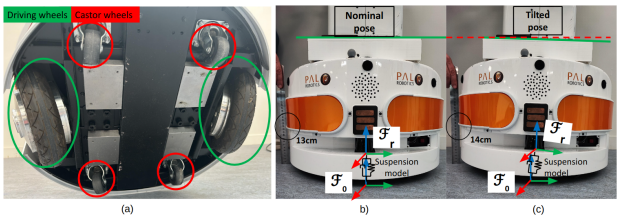

Fig. 3. Illustration of (a) the caster and driving wheels inducing flexibilities at the base of the robot, showing displacement of the base due to the suspension in the nominal robot configuration (b) and when the arm is fully extended on the left side (c).

In this section, we model each wheel as a simple spring-damper and establish the resulting relation between the motion of the base and the wrench applied by the ground on the robot. We assume that the driving wheels are blocked either by some brakes or by a static motor control. When the robot performs motion with the arm or is subjected to an external wrench, the suspension is excited and the base slightly moves with respect to the fixed reference frame as

illustrated in Fig.3.c. Then we denote the displacement of frame $\mathscr{F}_r$ with respect to $\mathscr{F}_0$ by a position vector $\mathbf{t} \in \mathbb{R}^3$ and a rotation matrix $\mathbf{R} \in SO(3)$. We denote by $\boldsymbol{\theta} \in \mathbb{R}^3$ the vector satisfying $\mathbf{R} = \exp([\boldsymbol{\theta}]_\times)$, where $[\boldsymbol{\theta}]_\times$ is the skew-symmetric matrix corresponding to the vector product by $\boldsymbol{\theta}$. As the displacement is of small magnitude, we may approximate $\mathbf{R}$ as follows: $\mathbf{R} \approx \mathbf{I} + [\boldsymbol{\theta}]_\times$.

For each wheel frame $\mathscr{F}_{w_i}$ presented in Fig.3.a, we denote by $\mathbf{r}_i$ the constant pose of the wheel frame origin expressed in $\mathscr{F}_r$. As $\mathscr{F}_r$ is displaced by the excitation, the wheel frame $\mathscr{F}_{w_i}$ also undergoes displacement. This local displacement, expressed in the fixed frame $\mathscr{F}_0$, can be calculated as:

$$\Delta\mathbf{r}_i \triangleq \mathbf{R}\mathbf{r}_i + \mathbf{t} - \mathbf{r}_i \approx \mathbf{t} + [\boldsymbol{\theta}]_\times \mathbf{r}_i = \mathbf{t} - [\mathbf{r}_i]_\times \boldsymbol{\theta} \quad (1)$$

Consider modeling each wheel as a suspension system consisting of a linear spring-damper and a torsional spring-damper. The local displacement of the wheel can be viewed as the displacement of the spring-dampers from their equilibrium position. The force exerted by the linear spring-damper has the following form:

$${}^0\mathbf{F}_i = \mathbf{K}_{\mathbf{t}i}\Delta\mathbf{r}_i + \mathbf{C}_{\mathbf{t}i}\Delta\dot{\mathbf{r}}_i \quad (2)$$

where $\mathbf{K}_{\mathbf{t}i} = diag(k_{tix},\ k_{tiy},\ k_{tiz})$ is the linear stiffness matrix, $\mathbf{C}_{\mathbf{t}i} = diag(c_{tix},\ c_{tiy},\ c_{tiz})$ is the linear damping matrix. Similarly, the moment exerted by the torsional spring-damper can be calculated as:

$${}^0\mathbf{M}_i = \mathbf{K}_{\boldsymbol{\theta}_i}\boldsymbol{\theta} + \mathbf{C}_{\boldsymbol{\theta}_i}\dot{\boldsymbol{\theta}} + \mathbf{r}_i \times {}^0\mathbf{F}_i \quad (3)$$

where $\mathbf{K}_{\boldsymbol{\theta}_i} = diag(k_{\theta ix},\ k_{\theta iy},\ k_{\theta iz})$ is the torsional stiffness matrix, $\mathbf{C}_{\boldsymbol{\theta}_i} = diag(c_{\theta ix},\ c_{\theta iy},\ c_{\theta iz})$ is the torsional damping matrix. The estimates of the ground reaction force and moment applied by the ground to the robot are calculated by the sum of all forces and moments due to the excitation in Equation (2), (3) and the nominal force ${}^0\mathbf{F}_\mathbf{N} = \{F_{Nx}, F_{Ny}, F_{Nz}\}$ and moment ${}^0\mathbf{M}_\mathbf{N} = \{M_{Nx}, M_{Ny}, M_{Nz}\}$ in the resting state. This is achieved by substituting Equation (1) into Equations (2) and (3):

$$\begin{aligned}
{}^0\hat{\mathbf{F}} =& {}^0\mathbf{F}_\mathbf{N} + \sum_{i=1}^{6}(\mathbf{K}_{\mathbf{t}i}(\mathbf{t} - [\mathbf{r}_i]_\times\boldsymbol{\theta}) + \mathbf{C}_{\mathbf{t}i}(\dot{\mathbf{t}} - [\mathbf{r}_i]_\times\dot{\boldsymbol{\theta}})) \\
{}^0\hat{\mathbf{M}} =& {}^0\mathbf{M}_\mathbf{N} + \sum_{i=1}^{6}(\mathbf{K}_{\boldsymbol{\theta}_i}\boldsymbol{\theta} + \mathbf{C}_{\boldsymbol{\theta}_i}\dot{\boldsymbol{\theta}} + [\mathbf{r}_i]_\times\mathbf{K}_{\mathbf{t}i}(\mathbf{t} - [\mathbf{r}_i]_\times\boldsymbol{\theta}) \\
&+ [\mathbf{r}_i]_\times\mathbf{C}_{\mathbf{t}i}(\dot{\mathbf{t}} - [\mathbf{r}_i]_\times\dot{\boldsymbol{\theta}})) \\
=& {}^0\mathbf{M}_\mathbf{N} + \mathbf{K}_{\boldsymbol{\theta}}\boldsymbol{\theta} + \mathbf{C}_{\boldsymbol{\theta}}\dot{\boldsymbol{\theta}} + \sum_{i=1}^{6}([\mathbf{r}_i]_\times\mathbf{K}_{\mathbf{t}i}(\mathbf{t} - [\mathbf{r}_i]_\times\boldsymbol{\theta}) \\
&+ [\mathbf{r}_i]_\times\mathbf{C}_{\mathbf{t}i}(\dot{\mathbf{t}} - [\mathbf{r}_i]_\times\dot{\boldsymbol{\theta}}))
\end{aligned} \quad (4)$$

In Equation (4), the parameters $\mathbf{K}_{\boldsymbol{\theta}_i}$ and $\mathbf{C}_{\boldsymbol{\theta}_i}$ representing the torsional spring and damper system at each individual wheel should be grouped into two sets of 3 generalized torsional parameters $\mathbf{K}_{\boldsymbol{\theta}} = \sum_{i=1}^{6}\mathbf{K}_{\boldsymbol{\theta}_i}$ and $\mathbf{C}_{\boldsymbol{\theta}} = \sum_{i=1}^{6}\mathbf{C}_{\boldsymbol{\theta}_i}$. This grouping acknowledges that these parameters are not individually observable and does not compromise the generality of the model.

We denote $\boldsymbol{\tau}_\mathbf{s} \in \mathbb{R}^{6N_s}$ as the concatenated vector representing measurements of ground reaction force and moments over N_s number of samples. A corresponding estimation vector of the same size $\hat{\boldsymbol{\tau}}_\mathbf{s}$ is calculated by Equation (4). We now can formulate the identification problem that estimates a set of parameters $\mathbf{P} = \{\mathbf{P}_{\mathbf{t}1}, ..., \mathbf{P}_{\mathbf{t}6}, \mathbf{P}_\theta, {}^0\mathbf{F}_\mathbf{N}, {}^0\mathbf{M}_\mathbf{N}\} \in \mathbb{R}^{48}$, where $\mathbf{P}_{\mathbf{t}i} = \{k_{t1x}, k_{t1y}, k_{t1z}, c_{t1x}, c_{t1y}, c_{t1z}\}$ are parameters of the linear spring-damper model at wheel $\mathcal{W}_i$, and $\mathbf{P}_\theta = \{k_{\theta x}, k_{\theta y}, k_{\theta z}, c_{\theta x}, c_{\theta y}, c_{\theta z}\}$ are parameters representing the generalized torsional spring-damper. The parameters set $\mathbf{P}$ is estimated by minimizing the error between the measurement vector of the ground reaction force and moment $\boldsymbol{\tau}_\mathbf{s}$ and its corresponding estimation vector $\hat{\boldsymbol{\tau}}_\mathbf{s}$ as:

$$\begin{aligned}
\min_{\mathbf{P}} \quad & \|\boldsymbol{\tau}_\mathbf{s} - \hat{\boldsymbol{\tau}}_\mathbf{s}(\mathbf{P})\|^2 \\
\text{s.t.} \quad & \mathbf{P}_{\mathbf{t}i} \geq 0, i = \{1, ..., 6\} \\
& \mathbf{P}_\theta \geq 0
\end{aligned} \quad (5)$$

B. Backlash and Non-geometric Phenomena In Joint Transmission System

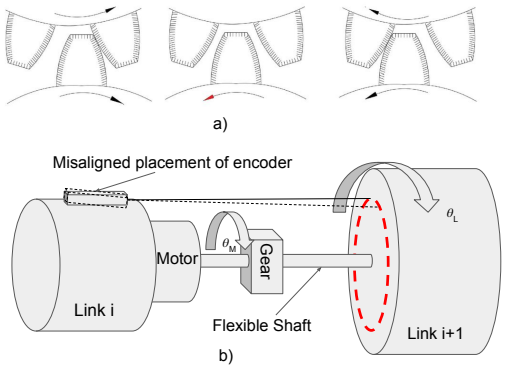

Fig. 4. Illustration of (a) the three phases of the backlash phenomenon [8] and (b) mounting of the drive chain including the motor the shaft and the relative and absolute encoders.

Fig. 4.a shows a simplified representation of the backlash phenomenon. It can be divided into 3 phases [8]. In the first phase, the driving gear and the driven gear teeth are in contact. In the second phase, the two teeth of two gears disengage and the driving gear travels across the gap while losing contact during the travel. In the third phase, the two teeth reengage, and a new contact is recovered on the opposite side. The gap, or the clearance between mating gears, is often referred to as the backlash phenomenon, which results in lost motion, or a lag between input and output movement when the direction of movement changes, and displayed as a non-linear hysteresis loop in input-output position graph. Ideally, the gap value is often modeled as a constant value. However, in some exceptional cases, for example, at the wrist of TIAGo, the two joints *arm_6* and *arm_7* are driven by a differential face gear system. This coupling would make the value of backlash gap at joint

arm_6 and *arm_7* would vary depending of the relative configuration of the face gears.

Moreover, as illustrated in Fig. 4.b, flexible shaft in the drive chain and imperfect mounting of the absolute encoders would contribute to the discrepancy between the input joint position θ_M and the output joint position θ_L, which are measured on the motor side and on the link side, respectively. Consequently, the observed gap at a joint would actually have different values depending on the torque τ applied to the joint and the joint configuration. Thus, it is crucial to model these behaviors incorporated with the backlash phenomenon.

We propose a model using a combination of sigmoid function and polynomials to describe these phenomena. The sigmoid function can represent the hysteresis loop of the backlash while maintaining the smoothness of the model [11]. This is of importance for the latter control and for the convergence of the identification method. The change of moving direction or the change in the sign of joint velocity is used as an activation in the sigmoid function subject to constant gain. Secondly, the polynomial function of joint position and torque, is used to approximate for the entangled phenomena including the flexibility of the drive chain and the misalignment of the encoder, and the effect of using differential gear. The hypothesized model of the discrepancy between the input and output positions at the joint k is presented as:

$$\Delta\hat{\theta}_{LM_k} = C_r(\theta_{M_k}, \tau_k)S(\dot{\theta}_{M_k}) + C_l(\theta_{M_k}, \tau_k)(1 - S(\dot{\theta}_{M_k})) \tag{6}$$

where

- polynomial $C_r(\theta_{M_k}, \tau_k) = \sum_{i=1}^{m}\sum_{j=1}^{n} A_{kij}\theta_{M_k}^i\tau_k^j$
- polynomial $C_l(\theta_{M_k}, \tau_k) = \sum_{i=1}^{m}\sum_{j=1}^{n} B_{kij}\theta_{M_k}^i\tau_k^j$
- A_k, B_k: coefficients of the polynomial functions
- τ_k: estimated joint torque at joint k
- m, n: orders of the polynomial
- sigmoid function $S(\dot{\theta}_{M_k}) = \frac{1}{1+e^{(-\rho\dot{\theta}_{M_k})}}$
- ρ: the gain of sigmoid function.

With N_{bl} measurements of input and output joint positions by dual encoders on the motor side and on the link side of 7 arm joints from joint *arm_1* to joint *arm_7*, the discrepancy between these two quantities can be calculated by subtraction and is represented by vector $\boldsymbol{\theta}_{\mathbf{LM}} \in \mathbb{R}^{7\times N_{bl}}$. An identification problem can be formulated to estimate the constant parameters set $\{\mathbf{A}, \mathbf{B}, \rho\}$ in the model Equation (6) as:

$$\begin{aligned} \min_{\mathbf{A},\mathbf{B},\rho} \quad & \|\boldsymbol{\Delta\theta}_{\mathbf{LM}} - \boldsymbol{\Delta}\hat{\boldsymbol{\theta}}_{\mathbf{LM}}(\mathbf{A}, \mathbf{B}, \rho)\|^2 \\ \text{s.t.} \quad & \rho > 0 \end{aligned} \tag{7}$$

C. Geometric Calibration

The geometric calibration is performed on the kinematic chain from frame $\mathscr{F}_b$ located at the base of the robot to frame $\mathscr{F}_g$ at its gripper, consisting of 8 joints including: {*torso*, *arm_1*, *arm_2*, *arm_3*, *arm_4*, *arm_5*, *arm_6*, *arm_7*}, by that order. Forward kinematics algorithm allows us to calculate the estimated pose $\hat{Y}_g \in \mathbb{R}^6$ of $\mathscr{F}_g$ expressed in the frame $\mathscr{F}_b$ as a function joint configuration $\mathbf{q} \in \mathbb{R}^8$ and a parameter vector $\boldsymbol{\Delta X} \in \mathbb{R}^{60}$ consisting of the sub-vector $\boldsymbol{\Delta X}_i = [\Delta p_{x_i}, \Delta p_{y_i}, \Delta p_{z_i}, \Delta\phi_{x_i}, \Delta\phi_{y_i}, \Delta\phi_{z_i}]$ representing the variation of the $i-th$ joint placement, and two other sub-vectors of 6 parameters describing the transformations from $\mathscr{F}_b$ to the first joint frame of the kinematic chain, and from its corresponding last joint frame to $\mathscr{F}_g$. By performing the first-order Taylor expansion, we approximate the linear relation between the variation vector $\boldsymbol{\Delta X}$ and the vector $\boldsymbol{\Delta}\hat{\mathbf{Y}}_{\mathbf{g}} \in \mathbb{R}^{6N_g}$ representing the resultant change of estimated poses $\boldsymbol{\Delta}\hat{\mathbf{Y}}_{\mathbf{g}}$ as:

$$\boldsymbol{\Delta}\hat{\mathbf{Y}}_{\mathbf{g}} = \mathbf{R}_{\mathbf{g}}\boldsymbol{\Delta X} \tag{8}$$

where

- N_g: number of measurements
- $\mathbf{R}_{\mathbf{g}} \in \mathbb{R}^{6N_g\times 60}$: observation matrix mapping $\boldsymbol{\Delta X}$ to $\boldsymbol{\Delta}\hat{\mathbf{Y}}_{\mathbf{g}}$

To remove the redundancy in the model, QR decomposition is applied on the matrix $\mathbf{R}_{\mathbf{g}}$, in which it would remove and group co-linear columns together forming a full-rank regressor matrix $\mathbf{R}_{\mathbf{b}} \in \mathbb{R}^{6N_g\times n_b}$ with its corresponding vector of grouped parameters $\boldsymbol{\Delta X}_{\mathbf{b}} \in \mathbb{R}^{n_b}$ [12] with n_b as the number of base parameters, expressed in the Equation (9).

$$\boldsymbol{\Delta}\hat{\mathbf{Y}}_{\mathbf{g}} = \mathbf{R}_{\mathbf{b}}\boldsymbol{\Delta X}_{\mathbf{b}} \tag{9}$$

The minimal set of identifiable parameters $\boldsymbol{\Delta X}_{\mathbf{b}}$ representing so-called base parameters, can be estimated by minimizing the squared error between the measured poses vector $\mathbf{Y}_{\mathbf{g}}$ and the corresponding estimated poses vector $\hat{\mathbf{Y}}_{\mathbf{g}}$, as presented in the Equation (10).

$$\min_{\boldsymbol{\Delta X}_{\mathbf{b}}} \quad \|\mathbf{Y}_{\mathbf{g}} - \hat{\mathbf{Y}}_{\mathbf{g}}(\boldsymbol{\Delta X}_{\mathbf{b}})\|^2 \tag{10}$$

In our study, Levenberg-Marquardt (LM) algorithm provided by numerical library *scipy* [13] was chosen to solve the least-squares problems in Equations (5), (7), (10) thanks to its effectiveness by combining the stability of the gradient descent method with the fast convergence of the Gauss-Newton method.

III. Experimentation

A. Experimental Setup

Experiments were conducted using a commercial version of the TIAGo robot, featuring a mobile base with 2 driving wheels, 4 caster wheels, a vertical-lifting 1-DOF torso, and a 7-DOF manipulating arm, a gripper. On-board sensors included relative encoders at each joint's motor side and absolute encoders at all joints' link side, except for the lifting torso joint.

To obtain accurate external kinematics data, a marker based stereophotogrammetric system (VICON, Vero v2.2, 120Hz) was used. Clusters of three retro-reflective markers were located at three locations on the robot to create frames at the gripper, the base, and the shoulder level. The external ground reaction wrench was measured below the robot using a laboratory grade force plate (AMTI OR6, 120Hz) with an

undeformable metallic material plate. Additionally, in order to create more dynamic excitation, an additional object with known dimensions and weight was added to the end-effector (see Fig. 2).

B. Protocol

Fig. 5. 21 optimal exciting postures, generated using FIGAROH [14], used to calibrate suspension and geometric models.

1) Geometric calibration with optimally exciting postures: The experimental protocol comprised three distinct phases. First, a classical geometric calibration was performed using the calibration toolbox FIGAROH [14] for parameter identification and optimal exciting posture generation.

As depicted in Fig. 5, 21 optimally exciting postures were used for a total experimental time of 5 minutes to calibrate the robot kinematic model. These postures were generated to maximize the determinant of the information matrix $\mathbf{I}(\mathbf{q}) = \mathbf{R}_b(\mathbf{q})^{\mathbf{T}}\mathbf{R}_b(\mathbf{q})$ of the kinematic calibration model, which is also equivalent to optimizing the optimality criterion O_1 [15]. In this first phase, the gripper position was expressed in the frame $\mathscr{F}_b$ created from the base markers. This was done to isolate the effect of the suspension as the base markers directly measured the base pose.

For each posture, absolute joint encoder readings and positional measures of the two marker sets at the base and the gripper were recorded. Using only the positional data of gripper marker, 31 geometric parameters have been identified, including 6 parameters representing transformation from base marker frame $\mathscr{F}_b$ to the robot reference frame $\mathscr{F}_0$. The geometric calibration yielded a RMSE of 3.3mm.

2) Identification of suspension system subjected to excitation motion: In the second phase, the robot was placed in the middle of the rigid force plate. During this phase, the robot maintained the lifting torso joint static while subjecting the arm to various exciting sinusoidal motions varied in: frequency between 0.2 - 1Hz, amplitude of 0.7rad, and directions exploring vertical, horizontal, and diagonal planes with respect to the floor. Both the resultant force and moment data

TABLE I

CALIBRATED GEOMETRIC PARAMETERS

	$x[m]$	$y[m]$	$z[m]$	$roll[rad]$	$pitch[rad]$	$yaw[rad]$
$base$	0.0191	-0.2005	-0.3147	0.0050	0.0103	0.0529
arm_1	0	0	0	-0.0010	-0.0030	0
arm_2	0.0020	0	0	-0.0003	0	0.0005
arm_3	-0.0027	0	0.0033	0.0005	0	-0.0120
arm_4	0	-0.0021	-0.0061	0	-0.0167	-0.0028
arm_5	0	-0.0109	0.0017	0	0.0470	0.01486
arm_6	0	-0.0333	0.0107	0	-0.0046	-0.0713
arm_7	0	0	0.0381	0	0	0
$gripper$	-0.0264	-0.0002	-0.1517	”	”	”

and the tracking and measurement of two marker clusters at the shoulder and the base were recorded simultaneously at 120 Hz by the software system NEXUS v2.12 [16]. Along with that, joint angles measured by onboard relative encoders were also recorded via a ROS node at 100 Hz, then synchronized with the resampled external data.

Utilizing previous results from the geometric calibration process, the transformation between the marker measurement frame $\mathscr{F}_b$ and the robot reference frame $\mathscr{F}_r$ could be established. Using the software Pinocchio [17], which implemented the rules of Lie theory and group in rigid-body dynamic modeling, allowed us to calculate the floating base pose and its kinematic derivatives, then to transform them in the same frame with dynamic measures by the force plate, and vice versa.

3) Backlash and discrepancy of encoder measures profiling: Finally, in the third phase, repetitive position-controlled motions were applied to all arm joints to discern the backlash model. These motions were designed to encompass a wide range of joint configurations and torque levels. For each run at a specific joint velocity (from $0.1rad/s$ to $1rad/s$, each joint was move incrementally by a step of 0.2rad from upper joint angle limit to lower joint angle limit and reverse the whole range. This process was repeated from all arm joints from *arm_1* to *arm_7*. By varying the frequency and amplitude of the motions, we ensured the excitation of different dynamic regimes, crucial for a comprehensive analysis of backlash and related phenomena.

Both readings from relative encoder on motor side and absolute encoder on driven link side were collected at 100 Hz by a ROS node for approximately 5 minutes per each joint. Kinematic derivatives were computed by center finite differentiation after a layer of low-pass filtering applied. Since there is no onboard torque sensor, joint torques were estimated using inverse dynamics algorithm. The parameters of the polynomial functions in Equation (6) can be identified by performing non-linear regression techniques.

IV. RESULTS AND DISCUSSION

A. Suspension Model Identification

The identified stiffness and damping parameters of the suspension model are presented table II. As not all parameters of retained multi-wheel suspension model can be observed, some parameters being linearly dependent upon one another, we set unobservable parameters to zero. Since there is a lack

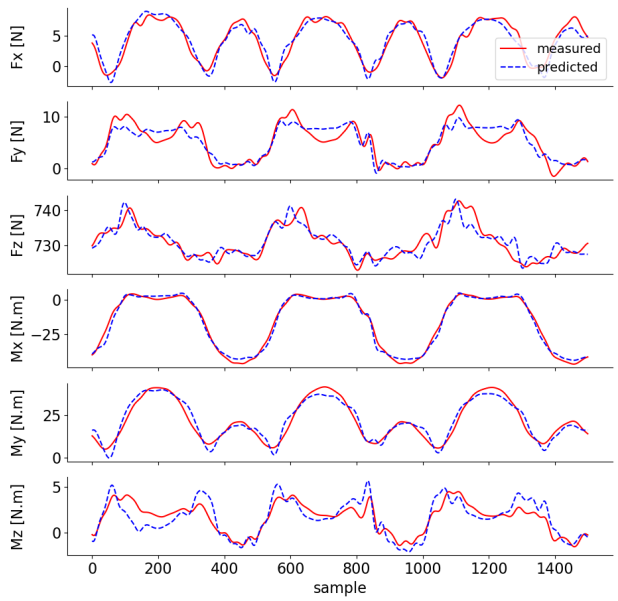

Fig. 6. Representative comparison of measured and estimated ground reaction forces and moments when using the identified suspension model.

of true nominal values for the suspension parameters, the evaluation of the identified model should be based on its prediction performance on a validation dataset.

TABLE II
IDENTIFIED PARAMETERS OF THE SPRING-DAMPER SUSPENSION MODEL

	K_{tx_i} $[\frac{N}{m}]$	K_{ty_i} $[\frac{N}{m}]$	K_{tz_i} $[\frac{N}{m}]$	C_{tx_i} $[\frac{N.s}{m}]$	C_{ty_i} $[\frac{N.s}{m}]$	C_{tz_i} $[\frac{N.s}{m}]$
WL	0.0	11498.47	323108.31	0.0	814.51	10722.72
WR	0.0	992.0	82919.08	0.0	698.77	5220.64
W_{BL}	6538.43	1.37	0.0	384.64	1381.43	0.0
W_{BR}	2136.63	4270.54	0.0	438.14	59.38	0.0
W_{FL}	6717.31	0.0	0.0	3730.7	0.0	26796.87
W_{FR}	4059.41	0.0	261792.46	526.1	0.0	11435.88
	$K_{\theta x}$ $[\frac{Nm}{rad}]$	$K_{\theta y}$ $[\frac{Nm}{rad}]$	$K_{\theta x}$ $[\frac{Nm}{rad}]$	$C_{\theta x}$ $[\frac{Nm.s}{rad}]$	$C_{\theta y}$ $[\frac{Nm.s}{rad}]$	$C_{\theta z}$ $[\frac{Nm.s}{rad}]$
	0.0	19252.57	127726.41	0.0	4949.37	10798.45
	F_{Nx} $[N]$	F_{Ny} $[N]$	F_{Nz} $[N]$	M_{Nx} $[Nm]$	M_{Ny} $[Nm]$	M_{Nz} $[Nm]$
	2.99	2.61	764.66	6.33	26.29	2.92

Fig. 6 shows a comparison of the predicted values of ground reaction forces and moments using the identified suspension model against the corresponding measured values on a separate validation dataset. In this figure, the corresponding RMSE were of 1.6N and 1.0N.m for forces and moments, respectively. The authors would argue that the high frequency fluctuations in F_y, F_z, M_z are not well estimated due to the small variation in the estimated transformation between the floating base $\mathscr{F}_0$ and $\mathscr{F}_b$ and/or to the fact that the robot inertial parameters were not properly identified. However, the proposed model appears sufficient to estimate any fluctuation with influential magnitudes to the robot.

B. Backlash And Non-geometric Phenomena Estimation

As mentioned previously in II-B, the gap between two gears would theoretically remain constant, but due to the flexibility of the transmission shaft and/or due to the misalignment of the encoder placements as well as the coupling in certain pairs of joints, the value of the backlash gap varies depending on the joint configuration and on the applied joint torque. In Fig. 7, the offsets between absolute encoder measures and relative encoder measures for each joint from arm_1 to arm_7 are represented in blue dots. The prediction of the backlash using the identified model are represented using red dots. The actual backlash values are observable on the z axis of these figures and in Fig.7.h.

The backlash detection and estimation are considered to be appropriate when the red dots are well-aligned with the blue dots in the 3D plots. As it can be seen from the Fig. 7, the erupt change in straight vertical line indicated the occurrence of the backlash, and the proposed model is able to track this behavior effectively using the approximation with sigmoid functions. The rest of the data can be described as two portions, upper and lower 3-D profiles. Each of these portion is expressed by a 5-th degree multivariate polynomial function of joint angles and joint torques. The coefficients of polynomials were obtained by solving the regression problem with the parametric model described by (6). The order of the polynomials was determined based on the benchmark of statistical performance criteria in a regression problem such as R-Squared value and RMS error, along with the required computation resource of the regression problem. Let us take the regression result on data of arm_6 as an demonstrative example, as shown in Fig. 8, the 5-th orders $[5, 5]$ on both polynomials fell into a sweet spot where it offered an R-Squared value of 0.9 and an RMSE of 0.003rad, while the computation would only take up to a few minutes, comparing to almost half of an hour of higher orders for similar criteria values.

The model performed well on most of the joints, except for the arm_7 joint. The jerky changes were indeed related to backlash behavior, but also its joint torque values could not be very well estimated due to the joint coupling, leading to inaccurate estimation of backlash gap. However, due to the fact that joint arm_7 is located at the end of the arm, the estimation error of backlash in joint arm_7 would contribute much less in magnitude compare to preceding joints.

C. Operational Positioning Accuracy Improvement

Lastly, after performing geometric calibration and complementary framework identifying the suspension model of the base and the non-geometric phenomena at the joints, the improvement of absolute positioning accuracy can now be assessed. Fig. 9 presents the distribution of the absolute errors between predicted values and measured values of marker position at the gripper expressed in the reference frame $\mathscr{F}_m$ of the motion capture system using different models mentioned in Fig. 1.

During the validation experiment, a periodic sinusoidal motion was executed on the arm joints. Table III describes

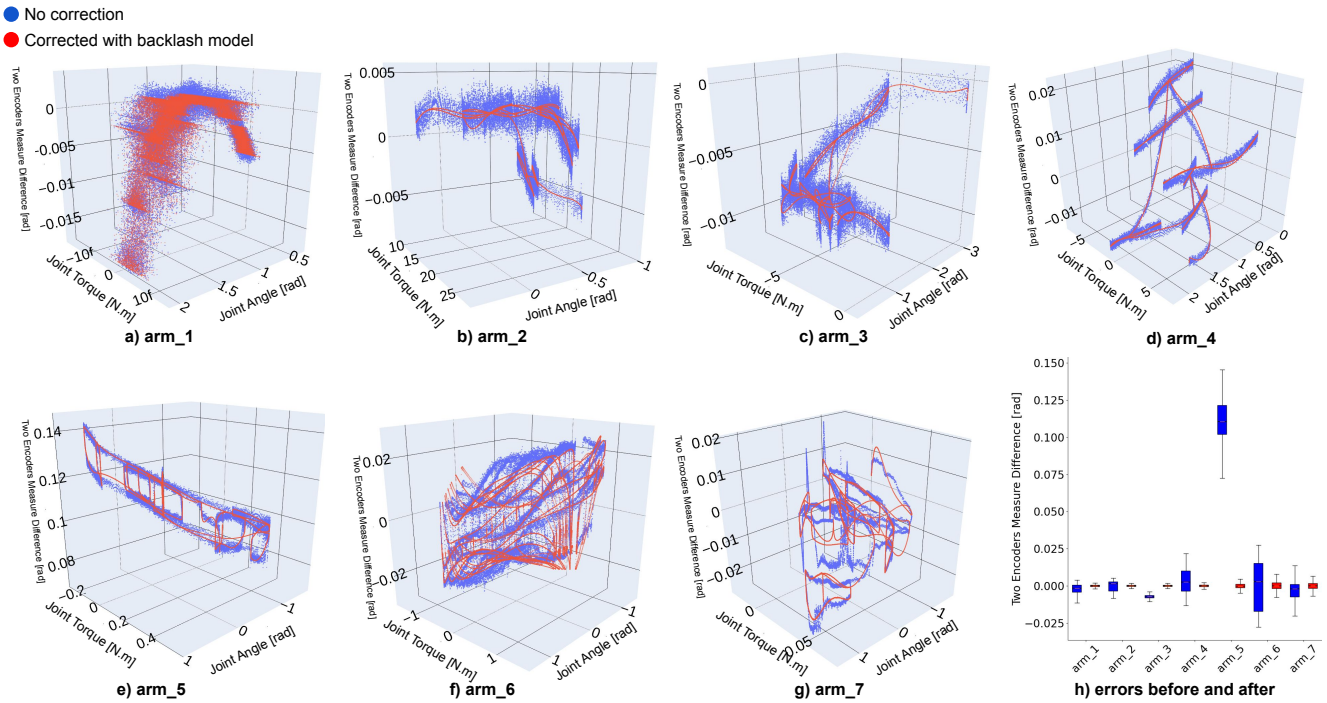

Fig. 7. Backlash estimation and offsets between two encoder values.

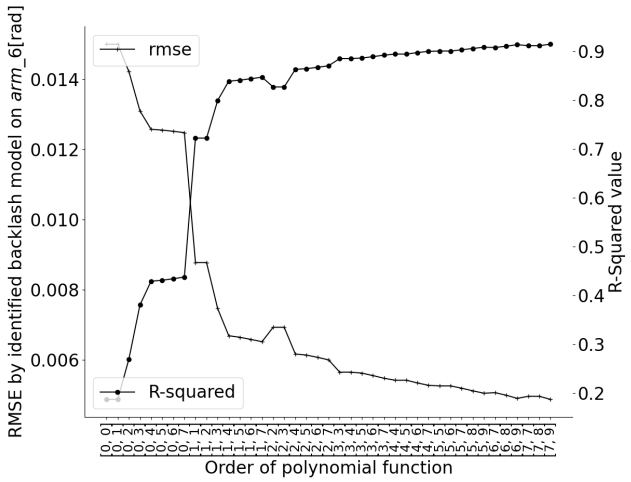

Fig. 8. Comparison of RMS error and R-Squared value between backlash models with increasing degree of polynomial.

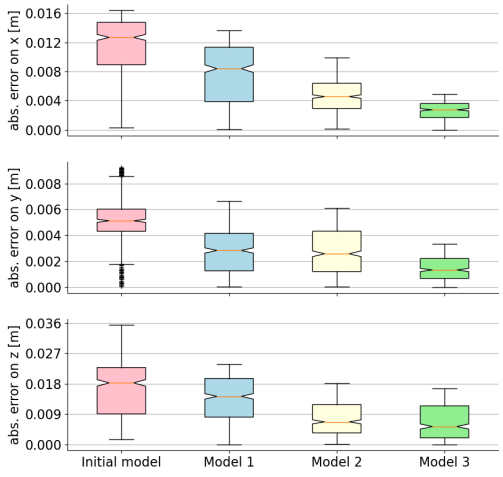

Fig. 9. Absolute errors between measured values and predicted values of the gripper marker position expressed in motion capture frame.

the 4 models used for comparison, and their corresponding RMSE as well as mean absolute error (MAE) on a validation dataset composed of 500 samples. Table III shows that the RMSE and MAE values are relatively close. It indicates that there is no particular outlier in our validation dataset since RMSE is often much more sensitive to outlier errors than MAE.

Clearly, it can be observed that the accuracy improved each time when an identified model is added. Firstly, the errors on the manufacturer's nominal model are relatively large with an average RMSE of 13.3mm for estimating the end-effector position. The added suspension model improves this result by diminishing the RMSE by 24% to 10.1mm. The key in drastically improving the accuracy was to use the geometrically calibrated model, that used the joint backlash/flexibility model as input data. In this case

TABLE III

AVERAGE RMSE AND MAE OF THE END-EFFECTOR POSITIONAL ESTIMATION ACCURACY

	positional RMSE [m]	positional MAE [m]	orientational RMSE [deg]	orientational MAE [deg]
Nominal model	0.0133	0.0111	8.57	7.89
Identified model 1	0.0101	0.0078	7.77	7.58
Identified model 2	0.0062	0.0049	4.92	3.81
Identified model 3	0.0057	0.0041	2.71	2.58

the RMSE was reduced by 57% to a RMSE of 5.7mm. In terms of orientation estimates, the RMSE reduced from 8.57deg to 2.71deg. Especially, a decrease of 44% in RMSE between model 2 and model 3, of which the non-geometric phenomena were identified in the latter, has clearly shown the significant impact of the large discrepancy at joint 5 due to non-geometric phenomena, even though it reduced only 8% in positional RMSE. This non-proportional error reduction can be explained by the fact that joint 5 is located closely to the end-effector.

V. CONCLUSION

In this paper, we have proposed three different models to improve mobile manipulator accuracy: a state-of-the-art calibrated kinematic model, a suspension of the robot's base model and non-linear joint model to reduce backlash, flexibility and encoder sensor misaligned mounting effects. The merit of this paper is to push further the use of a purely model based approach. It allows fast calculation for online trajectory generation and requiring little identification data, at contrary to purely data based approach. We demonstrated experimentally the improved accuracy of the absolute end-effector pose estimation of the mobile manipulator TIAGo the position and orientation error were reduced from 13.3mm to 5.7mm and 8.57deg to 2.71deg, respectively. On average, it is a reduction of 60% of the end-effector pose estimation error. Improvements given by the proposed approach could be crucial for projects where heavy objects or a large external wrench are to be used with a mobile manipulator robot while requiring high task accuracy. Indeed, these will emphasize the phenomenon observed in this paper. Nevertheless, even if the proposed models go beyond the literature, one can still observe some residual errors. It is likely that we reach the limit of the model-based approach with models that can be evaluated in real-time. Thus, to further compensate these errors future works will aim to combine a data driven approach together with the proposed model to cancel out the remaining residue. Indeed, it has been shown that using data driven approach to learn only over the remaining residue, observed after classical calibration, has the merit to reduce the number of samples required for learning [18] and reduces the size of the neural network.

REFERENCES

[1] C. Liu, Y. Huang, Y. Rong, G. Li, J. Meng, Y. Xie, and X. Zhang, "A novel extrinsic calibration method of mobile manipulator camera and 2d-lidar via arbitrary trihedron-based reconstruction," *IEEE Sensors Journal*, vol. 21, no. 21, pp. 24 672–24 682, 2021.

[2] M. Shah, R. Bostelman, S. Legowik, and T. Hong, "Calibration of mobile manipulators using 2d positional features," *Measurement*, vol. 124, pp. 322–328, 2018. [Online]. Available: https://www.sciencedirect.com/science/article/pii/S026322411830294X

[3] O. Limoyo, T. Ablett, F. Marić, L. Volpatti, and J. Kelly, "Self-calibration of mobile manipulator kinematic and sensor extrinsic parameters through contact-based interaction," in *2018 IEEE International Conference on Robotics and Automation (ICRA)*, 2018, pp. 4913–4920.

[4] N. Sarkar, R. Ellis, and T. Moore, "Backlash detection in geared mechanisms: Modeling, simulation, and experimentation," *Mechanical Systems and Signal Processing*, vol. 11, no. 3, pp. 391–408, 1997. [Online]. Available: https://www.sciencedirect.com/science/article/pii/S0888327096900825

[5] J. L. Stein and C.-H. Wang, "Automatic detection of clearance in mechanical systems: Experimental validation," *Mechanical Systems and Signal Processing*, vol. 10, no. 4, pp. 395–412, 1996. [Online]. Available: https://www.sciencedirect.com/science/article/pii/S088832709690028X

[6] M. Slamani, A. Nubiola, and I. A. Bonev, "Modeling and assessment of the backlash error of an industrial robot," *Robotica*, vol. 30, no. 7, p. 1167–1175, 2012.

[7] M. Ruderman, F. Hoffmann, and T. Bertram, "Modeling and identification of elastic robot joints with hysteresis and backlash," *IEEE Transactions on Industrial Electronics*, vol. 56, no. 10, pp. 3840–3847, 2009.

[8] E. Giovannitti, S. Nabavi, G. Squillero, and A. Tonda, "A virtual sensor for backlash in robotic manipulators," *Journal of Intelligent Manufacturing*, vol. 33, 04 2022.

[9] H.-C. Chuang, C.-W. Kung, L.-W. Chen, and S.-B. Jiang, "Nonlinear error correction for magnetic encoders," *IEEE Sensors Journal*, vol. 23, no. 9, pp. 9129–9135, 2023.

[10] V. Sujan and S. Dubowsky, "An optimal information method for mobile manipulator dynamic parameter identification," *IEEE/ASME Transactions on Mechatronics*, vol. 8, no. 2, pp. 215–225, 2003.

[11] Y. Yun, P. Agarwal, J. Fox, K. E. Madden, and A. D. Deshpande, "Accurate torque control of finger joints with ut hand exoskeleton through bowden cable sea," in *2016 IEEE/RSJ International Conference on Intelligent Robots and Systems (IROS)*, 2016, pp. 390–397.

[12] M. Gautier, "Numerical calculation of the base inertial parameters of robots," in *Proceedings., IEEE Int. Conf. Robot. Autom.*, 1990, pp. 1020–1025 vol.2.

[13] P. Virtanen, R. Gommers, T. E. Oliphant, M. Haberland, T. Reddy, D. Cournapeau, E. Burovski, P. Peterson, W. Weckesser, J. Bright, S. J. van der Walt, M. Brett, J. Wilson, K. J. Millman, N. Mayorov, A. R. J. Nelson, E. Jones, R. Kern, E. Larson, C. J. Carey, İ. Polat, Y. Feng, E. W. Moore, J. VanderPlas, D. Laxalde, J. Perktold, R. Cimrman, I. Henriksen, E. A. Quintero, C. R. Harris, A. M. Archibald, A. H. Ribeiro, F. Pedregosa, P. van Mulbregt, and SciPy 1.0 Contributors, "SciPy 1.0: Fundamental Algorithms for Scientific Computing in Python," *Nature Methods*, vol. 17, pp. 261–272, 2020.

[14] D. V. T. Nguyen, V. Bonnet, S. Maxime, M. Gautier, P. Fernbach, and F. Lamiraux, "FIGAROH: a Python toolbox for dynamic identification and geometric calibration of robots and humans," in *IEEE-RAS International Conference on Humanoid Robots*, Austin (TX), United States, Dec. 2023. [Online]. Available: https://laas.hal.science/hal-04234676

[15] J.-H. Borm and C.-H. Menq, "Determination of optimal measurement configurations for robot calibration based on observability measure," *The International Journal of Robotics Research*, vol. 10, pp. 51 – 63, 1991.

[16] Vicon, "What's new in vicon nexus 2.12?" 2023, accessed: 2024-10-08. [Online]. Available: https://help.vicon.com/space/Nexus212/11241032/What's+new+in+Vicon+Nexus+2.12%253F

[17] J. Carpentier, G. Saurel, G. Buondonno, J. Mirabel, F. Lamiraux, O. Stasse, and N. Mansard, "The pinocchio c++ library – a fast and flexible implementation of rigid body dynamics algorithms and their analytical derivatives," in *IEEE International Symposium on System Integrations (SII)*, 2019.

[18] C. Landgraf, K. Ernst, G. Schleth, M. Fabritius, and M. F. Huber, "A hybrid neural network approach for increasing the absolute accuracy of industrial robots," in *2021 IEEE 17th International Conference on Automation Science and Engineering (CASE)*, 2021, pp. 468–474.